

**Theoretical study of current-voltage characteristics of carbon nanotube wire functionalized  
with hydrogen atoms**

FUENO Hiroyuki, KOBAYASHI Yoshikazu & TANAKA Kazuyoshi\*

*Department of Molecular Engineering, Graduate School of Engineering, Kyoto University,*

*Nishikyo-ku, Kyoto 615-8510, Japan*

**Abstract**

A functionalized single-walled carbon nanotube (SWCNT) of a finite length with a ring-like hydrogenation around its surface is designed toward fabrication of a molecular field-effect transistor (FET) device. The molecular wire thus designed is equipped with a quantum dot inside, which is confirmed by theoretical analysis for electronic transport. In particular, the current-voltage ( $I$ - $V$ ) characteristics under influence of the gate voltage are discussed in details.

**single-walled carbon nanotube, molecular field-effect transistor, molecular wire, electron transport**

\*Corresponding author (email: ktanaka@moleng.kyoto-u.ac.jp)

## 1 Introduction

Carbon nanotube (CNT) is a well known allotrope of carbon material and has been attracting much attention as one of the principal parts for making molecular electronic devices [1]. For instance, there is a possibility to make high-speed transistor due to ballistic conduction characteristics when a single CNT chain is used [2].

A model structure of molecular field-effect transistor (FET) is shown in Fig. 1 as one of the nanoelectronic devices. The molecular FET is comprised of a source electrode to supply an electron, a drain electrode to accept the electron, a molecular wire equipped with the site acting as quantum dot to characterize the electric current between the both electrodes, and a gate electrode to afford electric field effect to the quantum dot [3]. Quantum dot in CNT has thus been rather eagerly studied [4-14]. An early study by Postma *et al.* has even utilized the two defects (bending points) in a single-walled CNT (SWCNT) chain as the energy barrier to generate a quantum dot for fabrication of a single electron transistor (SET) [4].

However, it will be desirable that the quantum dot does not come from such accidental fact like defects. In the present study, we theoretically design a more sophisticated and chemically possible functionalization to divide an SWCNT chain by two energy barriers so as to generate the molecular wire with a quantum dot inside as shown in Fig. 1, and then theoretically investigate the electronic transport behavior of thus designed system. In particular, the current-voltage ( $I$ - $V$ ) characteristics of the system under the application of the gate voltage are also to be analyzed to check the resonant tunneling for the electron flow.

## 2 Computational method and models

The molecular FET system is set up as shown in Fig. 2, which consists of the left and right electrodes (**L** and **R**) having chemical potential,  $\mu_L$  and  $\mu_R$ , respectively, and the central region **C**

with several discrete orbital energy levels. This discreteness is introduced by separation of a long single molecule such as a CNT chain with two energy barriers to isolate the region **C**. How to make the energy barriers will be described a bit later.

The transport calculation was performed using the non-equilibrium Green's function (NEGF) method [3] based on the density functional theory (DFT) using the Perdew-Zunger local density approximation parameterization (LDA-PZ) [15] with the single zeta basis function [16]. The Transiesta-C 1.3 program package [17, 18] was employed for the present calculation.

Since the thorough prescription of the computation is given elsewhere [19], some essence of the formulation is noted in the below. The NEGF  $G$  is given by

$$G(\varepsilon) = [\varepsilon - H - \Sigma_L - \Sigma_R]^{-1} \quad (1)$$

where  $\varepsilon$  and  $H$  represent the one-electron energy and the Hamiltonian in the central region, respectively, defined in Fig. 2. Within the DFT framework employed in the present study, this Hamiltonian is written as

$$H = -\frac{\hbar^2}{2m}\nabla^2 + V^{\text{eff}}[n] \quad (2)$$

$V^{\text{eff}}[n]$  signifying the effective potential consisting of the ion potential, the Hartree potential, and the exchange correlation potential as usual in the DFT scheme, and  $[n]$  symbolically representing the electron density.  $\Sigma_{L(R)}$  stands for the self-energy expressing effect of the combination of the electrodes and the central region of molecular wire with its real part representing the shift of energy levels and its imaginary part their broadening. The self-energy  $\Sigma_{L(R)}$  is written in terms of the surface Green's function of the electrodes  $g_{L(R)}$  and the interaction term  $V_{L(R)}$  between the electrode and the central molecular region as

$$\Sigma_{L/R} = V_{L/R}^\dagger g_{L/R} V_{L/R} \quad (3)$$

The transmission probability is calculated by

$$\mathbf{T}(\varepsilon) \equiv \text{Tr}[(\text{Im}\Sigma_L(\varepsilon))G^\dagger(\varepsilon)(\text{Im}\Sigma_R(\varepsilon))G(\varepsilon)] \quad (4)$$

where Tr and Im signify the trace of matrix and the imaginary part, respectively. This quantity is

important since it gives the electric current value as

$$I(V) = G_0 \int_{-\infty}^{\infty} d\varepsilon \{ [n_F(\varepsilon - \mu_L) - n_F(\varepsilon - \mu_R)] \times \mathbf{T}(\varepsilon) \} \quad (5)$$

with the conductance quantum

$$G_0 \equiv \frac{2e^2}{h} \quad (6)$$

and the Fermi distribution function  $n_F$ .

As a matter of course, both the  $\mu_L$  and  $\mu_R$  values are equal at the source-drain (bias) voltage  $V_{sd} = 0$  V, where electric current does not occur. However, this voltage balance alters when positive  $V_{sd}$ , for example, is applied as shown in Fig. 2. The electrons in the both electrodes are filled up to  $\mu_L$  and  $\mu_R$  and the average of these is taken as the zero energy for  $\varepsilon$ . The potential difference between  $\mu_L$  and  $\mu_R$  is denoted as the bias window, and an electron drifts from the right (**R**) to the left (**L**) electrodes via the energy levels of the region **C** (the electric current  $I_{sd}$  flows from **L** to **R**). Transmission probability  $\mathbf{T}$  expresses this electron drift ratio through the entire molecular wire. In the present calculation, actual integration for the current formula  $I(V)$  in Eq.(2) was restricted in the range of  $\mu_L$  to  $\mu_R$  apart from the range  $-\infty$  to  $+\infty$ , which is considered to be enough.

A metallic SWCNT(6, 6) of a finite length was employed throughout this study. Two kinds of systems in Figs. 3(a) and (b) are considered. Note also that in the present study two CNT's with the half infinite lengths were employed as the electrodes instead of the conventional metallic electrodes.

These regions **L** and **R** are represented by two CNT rings, and the region **C** by six rings as shown in Fig. 3(a). Let us call this simple system **CNT**. On the other hand, Fig. 3(b) called **H-CNT** has the structure in which the regions **L** and **R** consist of two CNT rings, whereas the region **C** of twelve rings with the  $z_1$  and  $z_2$  peripheries each on which twelve hydrogen atoms are added around the CNT surface to isolate the  $z_H$  region. The position of the hydrogen atoms are also illustrated in Fig. 4. Introduction of these twenty-four hydrogen atoms makes the  $\sigma$ -bonded

zone due to the  $sp^3$  hybridization at  $z_1$  and  $z_2$  rings, which act as the energy barriers to turn the  $z_H$  region into a quantum dot in **H-CNT**.

### 3 Results and discussion

Calculated  $I_{sd} - V_{sd}$  characteristics of **CNT** and **H-CNT** (inset) are shown in Fig. 5. There are three remarkable features: (1) The ohmic behavior is seen up to 1.6 V for **CNT**, (2) a current peak appears at 1.6 V for **H-CNT** accompanied by the succeeding negative differential resistance (NDR) signifying that current falls down with increase in the applied voltage, and (3) the  $I_{sd} - V_{sd}$  curve saturates at about 1.8 V for **CNT**. It is also seen that the current in **H-CNT** is in the order of one hundredth of that of **CNT** for  $V_{sd}$  ranging from 1 to 2 V. In what follows these will be analyzed in detail by examining the electronic structures in terms of transmission spectra, band structures, and molecular orbitals.

The transmission spectra of **CNT** and **H-CNT** with different  $V_{sd}$  are shown in Figs. 6(a) and (b), respectively. The energy  $\varepsilon$  corresponds to that in Fig. 2. The origin of energy  $\varepsilon$  is the average chemical potentials (or Fermi energies) of  $\mu_L$  and  $\mu_R$  as described above. The transmission spectra area surrounded by dashed triangular lines corresponds to those within the bias window.

For **CNT** all the transmission spectra remain 2 in the bias-window range up to 1.6 V where the  $I_{sd} - V_{sd}$  characteristics become ohmic since the bias window width is proportional to  $V_{sd}$ . This suggests that **CNT** behaves as a good molecular wire in itself. On the other hand, these spectra for **H-CNT** are generally smaller than 2 except for several sharp peaks. In particular, there is a small peak at  $V_{sd} = 1.6$  V as pointed by an arrow in the range of the bias window. This small peak corresponds to the current peak at  $V_{sd} = ca. 1.6$  V in the inset of Fig. 5 at which the NDR appears.

In addition, there appears, in the range of the bias window of **CNT**, a drop of the transmission spectra down to less than 2 at  $V_{sd} = 1.8$  V as shown in Fig. 6(a). This feature is to be explained by

considering the band structure as follows: Figure 7 shows the band structures of semi-infinite regions **R** and **L** calculated at  $V_{sd} = 2$  V along with the transmission spectrum depicted from Fig. 6(a) with  $\mu_R$  and  $\mu_L$  being 1 eV and -1 eV, respectively. The solid lines of the band structures contribute to electric current flowing through the region **C**. When  $\varepsilon$  is equal to 0 eV in Fig. 7, the transmission spectrum shows the value 2 since there are “two” band branches in both the regions **R** and **L** signifying the electronic state is 2 in the both electrodes. On the other hand, for  $\varepsilon$  of 1.5 eV, the band branch of the left electrode (**L**) becomes “one” so that the transmission spectrum shows the value 1. This situation is able to explain the decreasing tendency of the gradient of the  $I_{sd} - V_{sd}$  curve seen in Fig. 5. Similar gradient behavior has also been observed experimentally [20], the reason of which was attributed to the phonon-electron coupling. However, the present study indicates that invoking of the phonon-electron coupling is not necessarily indispensable.

The unoccupied orbitals of the molecular projected self-consistent Hamiltonian (MPSH) [17, 18] of **CNT** shown in Figs. 8(a) and (b) have the orbital energies of -0.01 and 0.01 eV, respectively. These are delocalized over the central region and contribute to electric current at  $V_{sd} = 0.2$  V. On the other hand, as to **H-CNT**, it is seen in Fig. 8(c) that the unoccupied orbital whose energy is 0.63 eV is confined in the  $Z_H$  region under the condition of  $V_{sd} = 1.6$  V. It is thus understood that the  $Z_H$  region behaves as a quantum well for **H-CNT**.

Figure 9 shows the gate voltage ( $V_g$ ) dependencies of  $I_{sd} - V_{sd}$  characteristics. Note that the orbital energy level in the region **C** can be controlled by applying  $V_g$ . It is seen that in Fig. 9(a) for **CNT** the change in  $V_g$  does not give remarkable effect to the  $I_{sd} - V_{sd}$  characteristics, since there is no quantum dot in **CNT**. On the other hand for **H-CNT**, the  $I_{sd} - V_{sd}$  characteristics show typical oscillation tendency and increase in the number of peaks upon the change in  $V_g$ . This obviously signifies the resonant tunneling in which the orbital energy levels are made to match to those of the outer wire portions by changing the gate voltage. Moreover, Fig. 10 shows the  $V_g$

dependency of the transmission spectra for **H-CNT** at  $V_{sd} = 0$  and 2 V, respectively. At  $V_{sd} = 0$  V, the spectra shift to slightly higher energy upon application of  $V_g$ . On the other hand, at  $V_{sd} = 2$  V, the spectral peaks do not shift by  $V_g$ . This suggests that when we use **H-CNT** as a molecular device, the effect of  $V_g$  becomes larger with the smaller  $V_{sd}$ .

The electron density  $\rho$  of the **C** region is given by

$$\rho = \frac{1}{\pi} \text{Im} G \quad (7)$$

which depends on the space coordinates,  $V_{sd}$ , and  $V_g$  values. Let us further define the electron density difference  $\Delta\rho$  by the difference of the averaged  $\rho$  values on the  $20\text{\AA} \times 20\text{\AA}$  plane perpendicular to the tube axis of CNT at the **C** region for  $V_g = 0.5$  and 0 V at constant  $V_{sd} = 2$  V. In Figs. 11(a) and (b) are shown the  $\Delta\rho$  values as the function of  $z$  for **CNT** and **H-CNT**, respectively. It is seen that the  $\Delta\rho$  value of **CNT** is generally smaller than that of **H-CNT**, which signifies that  $\rho$  does not change largely in **CNT** upon the change in  $V_g$  compared with **H-CNT**. It is of interest for **H-CNT** that  $\Delta\rho$  is positive in the  $Z_H$  region but negative outside. This means that  $\rho$  increases by applying  $V_g$  and electron is accumulated and confined in the  $Z_H$  region. This again visualizes that characteristics of quantum dot of the  $Z_H$  region act as a quantum dot by the addition of hydrogen atoms to the side wall of SWCNT and with application of the gate voltage.

In conclusion, we have theoretically examined the basic  $I_{sd}$ - $V_{sd}$  characteristics of molecular FET using an SWCNT wire of a finite length. Design of introducing quantum dot amid the CNT wire has successfully been performed by introducing hydrogen atoms regularly added around its surface. The resonant tunneling behavior of the electrons across the quantum dot has also been confirmed by applying the gate voltage. Finally, it is obviously desirable to fabricate the actual molecular FET in the near future.

**Words to Professor Wang Fosong:** It is our great honor and pleasure to dedicate our article to this special issue in *Science China Chemistry* celebrating your 80 years' birthday. One of us (KT) has been acquainted with you from 1980's during your days in Changchung Institute for Applied Chemistry and is quite proud of that. We eagerly wish you be healthy and continue to contribute to your Country and the whole world.



## References

- 1 Anantram MP, Léonard F. Physics of carbon nanotube electronic devices. *Rep. Prog. Phys.*, 2006, 69: 507-561
- 2 Tans SJ, Devoret MH, Dai H, Thess A, Smalley RE, Geerligs LJ, Dekker C. Individual single-wall carbon nanotubes as quantum wires. *Nature*, 1997, 386: 474-477
- 3 Datta S. Quantum Transport – Atom to Transistor. Cambridge University Press, Cambridge, 2005
- 4 Postma HWCh, Teepen T, Yao Z, Grifoni M, Dekker C. Carbon nanotube single-electron transistors at room temperature. *Science*, 2001, 293: 76-79
- 5 Rocha CG, Dargam TG, Latgé A. Carbon nanotube quantum dots. *Phys. Stat. Sol. (b)*, 2002, 232: 37-43
- 6 Liu H, Tao Y. Size effect of quantum conductance in single-walled carbon nanotube quantum dots. *Eur. Phys. J. B*, 2003, 36: 411-418
- 7 Ren W, Wang J. Electronic transport through single-wall nicked carbon nanotubes. *Phys. Rev. B*, 2004, 69: 33306(4).
- 8 Kim Y-H, Chang KJ. Electron transport through quantum-dot states of n-type carbon nanotubes. *Appl. Phys. Lett.*, 2002, 81: 2264-2266
- 9 Tsuya D, Suzuki M, Aoyagi Y, Ishibashi K. Quantum dots and their tunnel barrier in semiconducting single-wall carbon nanotubes with a p-type behavior. *Jpn. J. Appl. Phys.*, 2005, 44: 2596-2599
- 10 Biercuk MJ, Garaj S, Mason N, Chow JM, Marcus CM. Gate-defined quantum dots on carbon nanotubes. *Nano Lett.*, 2005, 5: 1267-1271
- 11 Gräber MR, Coish WA, Hoffmann C, Weiss M, Furer J, Oberholzer S, D. Loss D, Schönenberger C. Molecular states in carbon nanotube double quantum dots. *Phys. Rev. B*,

- 2006, 74: 75427(5)
- 12 Cleuziou J-P, Wernsdorfer W, Andergassen S, Florens S, Bouchiat V, Ondarçuhu Th, Monthieux M. Gate-tuned high frequency response of carbon nanotube Josephson junctions. *Phys. Rev. Lett.*, 2007, 99: 117001(4)
  - 13 Holm JV, Jørgensen HI, Grove-Rasmussen K, Paaske J, Flensberg K, Lindelof PE. Gate-dependent tunneling-induced level shifts observed in carbon nanotube quantum dots. *Phys. Rev. B*, 2008, 77: 161406(4)
  - 14 Anders FB, Logan DE, Galpin MR, Finkelstein G. Zero-bias conductance in carbon nanotube quantum dots. *Phys. Rev. Lett.*, 2008, 100: 86809(4)
  - 15 Perdew JP, Zunger A. Self-interaction correction to density-functional approximations for many-electron systems. *Phys. Rev. B*, 1981, 23: 5048-5079
  - 16 Soler JM, Artacho E, Gale JD, Gracia A, Junquera J, Ordejón P, Sánchez-Portal D. The SIESTA method for ab initio order-N materials simulation. *J. Phys.: Condens. Matter*, 2002, 14: 2745-2779
  - 17 Brandbyge M, Mozos J-L, Ordejón P, Taylor J, Stokbro K. Density-functional method for nonequilibrium electron transport. *Phys. Rev. B*, 2002, 65: 165401(17)
  - 18 Taylor J, Guo H, Wang J. Ab initio modeling of quantum transport properties of molecular electronic devices. *Phys. Rev. B*, 2001, 63: 245407(13)
  - 19 Stokbro K, Taylor J, Brandbyge M, Guo H. Ab-initio non-equilibrium Green's function formalism for calculating electron transport in molecular devices. *Lecture Notes in Physics*, 2005, 680: 117-151(G. Cuniberti, G. Fagas, and K. Richter, eds.) Springer, Berlin.
  - 20 Yao Z, Kane CL, Dekker C. High-field electrical transport in single-wall carbon nanotubes. *Phys. Rev. Lett.*, 2000, 84: 2941-2944

## Figure Captions

- Figure 1 A conceptual diagram of molecular FET.
- Figure 2 The molecular FET system considered in the present study.
- Figure 3 Structures of (a) **CNT** and (b) **H-CNT** employed in the present research.
- Figure 4 Generation of a quantum dot in **H-CNT** consisting of an SWCNT (6, 6) of a finite length functionalized with twenty-four hydrogen atoms. The two arrows indicate the peripheries  $z_1$  and  $z_2$  on which are added the hydrogen atoms .
- Figure 5 The  $I_{sd} - V_{sd}$  characteristics of **CNT**, where the inset shows that of **H-CNT**.
- Figure 6 Transmission spectra  $\mathbf{T}(\varepsilon)$  of (a)**CNT** and (b)**H-CNT**.
- Figure 7 The band structures of the **L** and **R** electrodes with the transmission spectrum for **CNT**.
- Figure 8 Orbital patterns by the MPSH (see text) with the orbital energies of (a) -0.01 and (b) 0.01 eV contributing to electronic current at  $V_{sd} = 0.2$  V for **CNT** and of (c) 0.63 eV at  $V_{sd} = 1.6$  V for **H-CNT**.
- Figure 9  $V_g$  dependencies of the  $I_{sd} - V_{sd}$  characteristics for (a) **CNT** and (b) **H-CNT**.
- Figure 10  $V_g$  dependencies of the transmission spectra for **H-CNT** at (a)  $V_{sd} = 0$  V and (b)  $V_{sd} = 2$  V.
- Figure 11 Electron density difference  $\Delta\rho$  for (a) **CNT** and (b) **H-CNT** at  $V_g = 0.5$  and 0 V with  $V_{sd} = 2$  V.

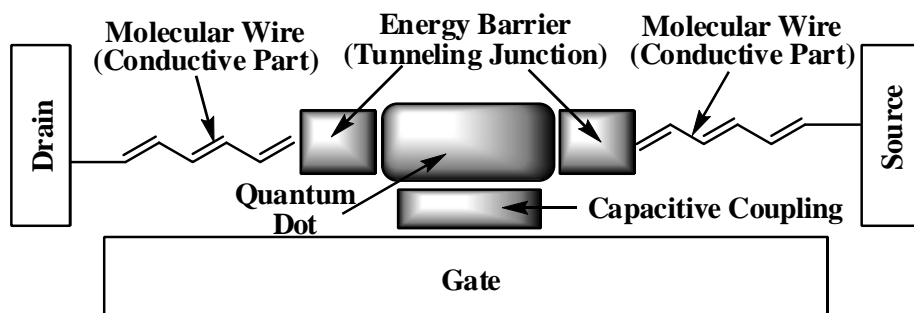


Figure 1

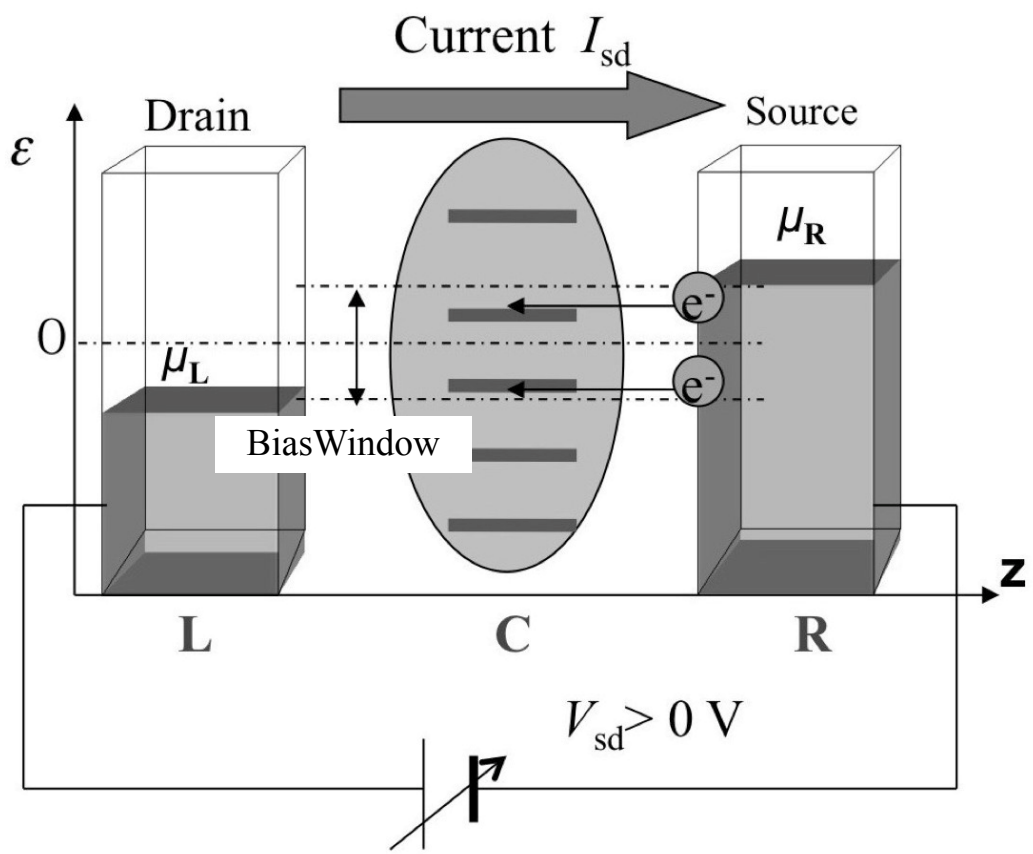


Figure 2

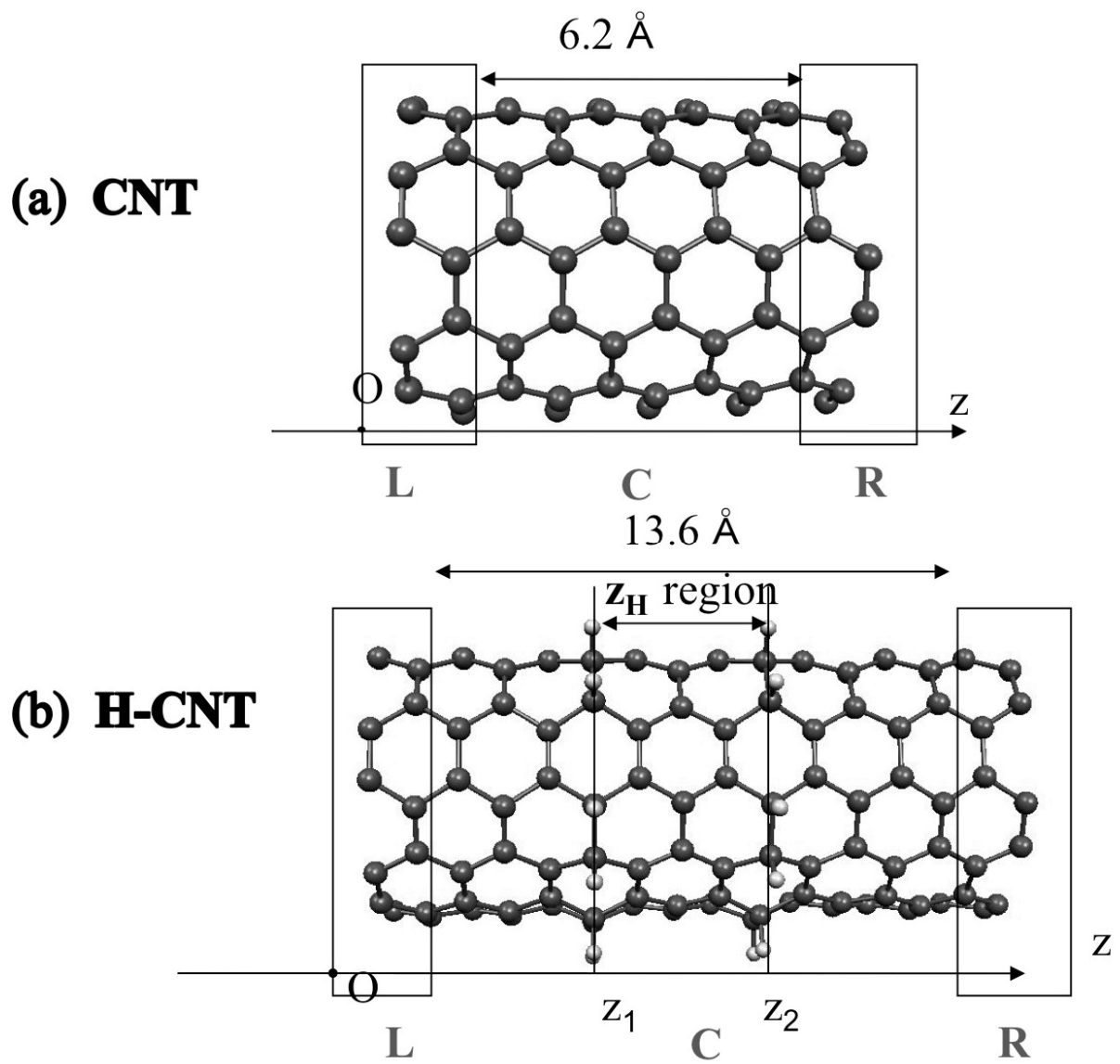


Figure 3

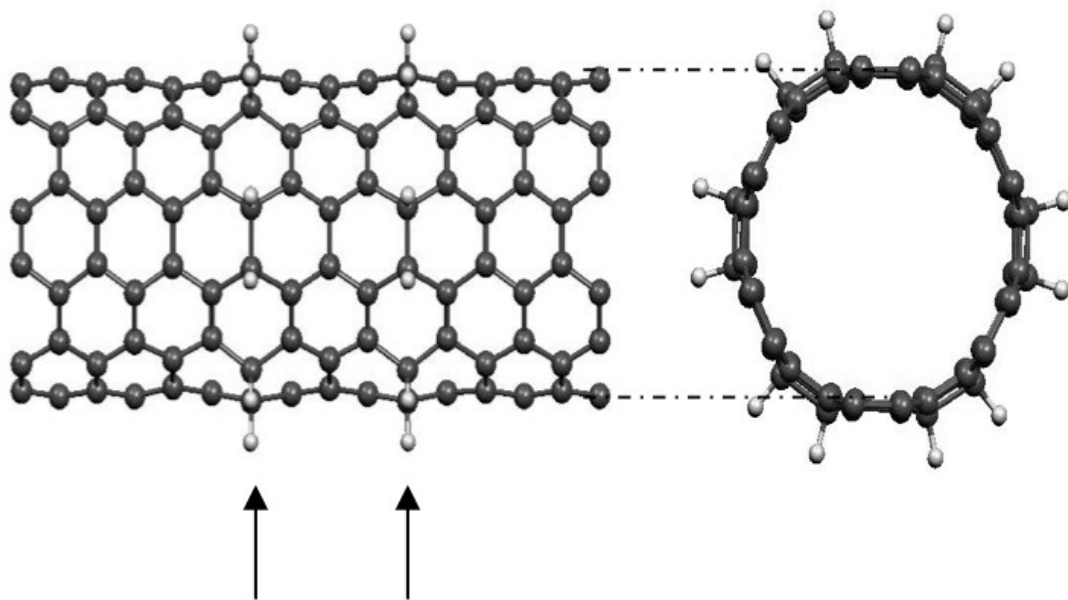


Figure 4

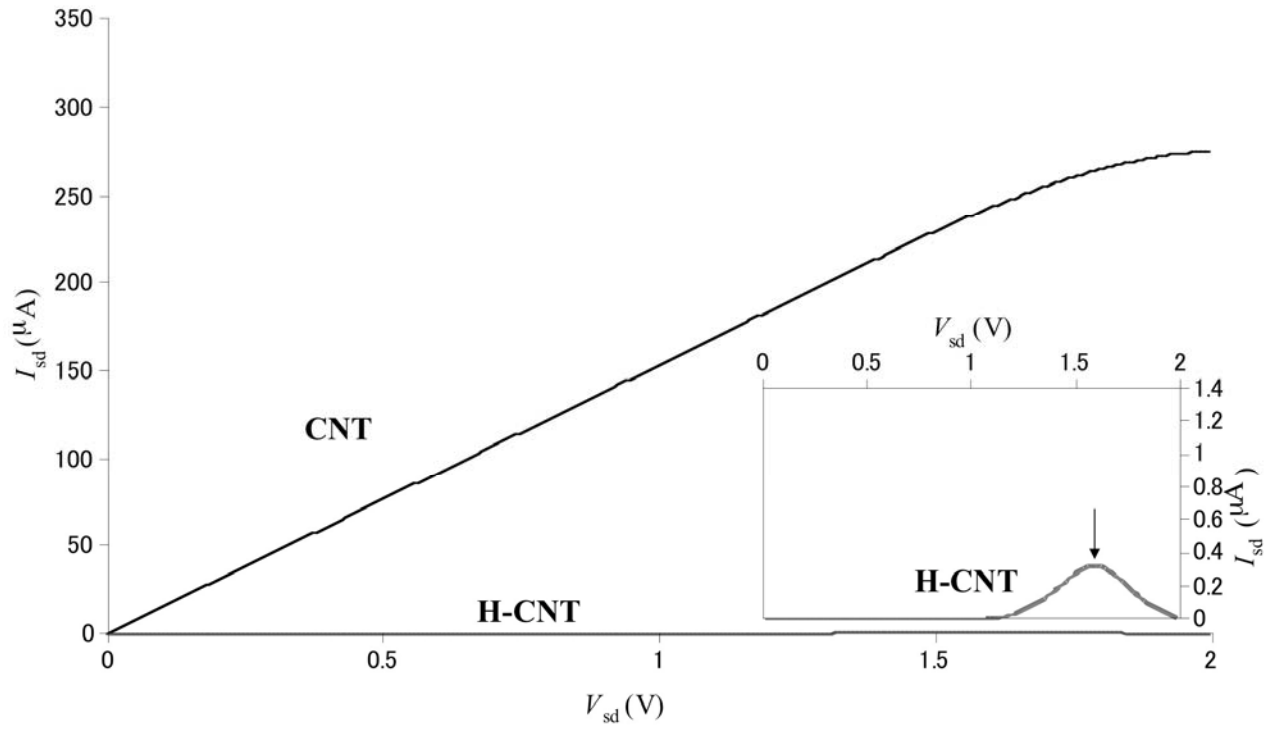


Figure 5



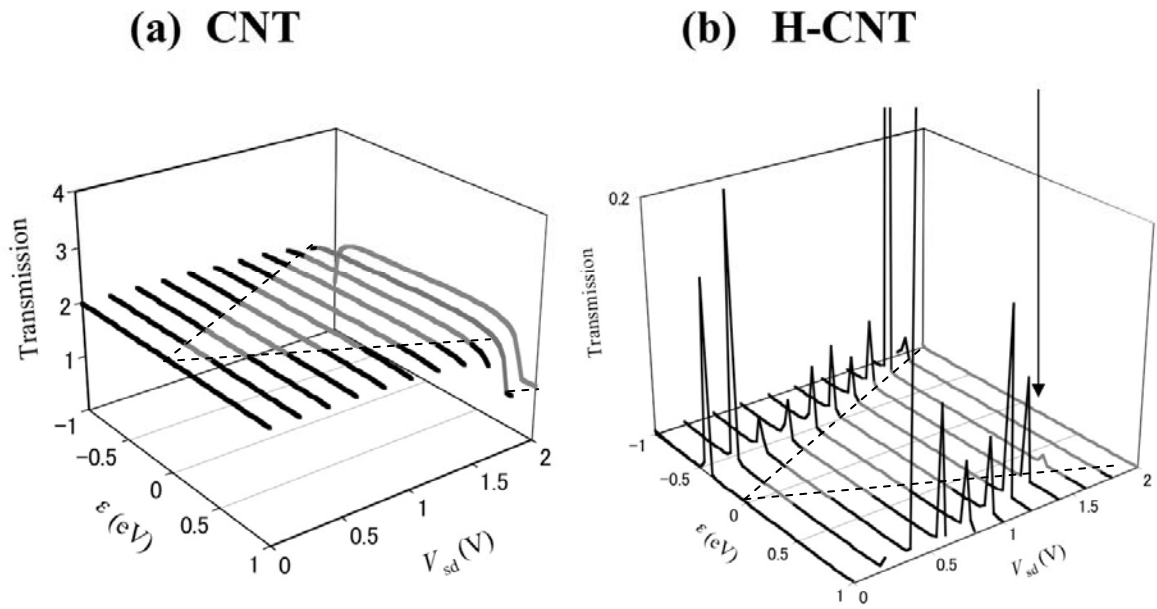


Figure 6

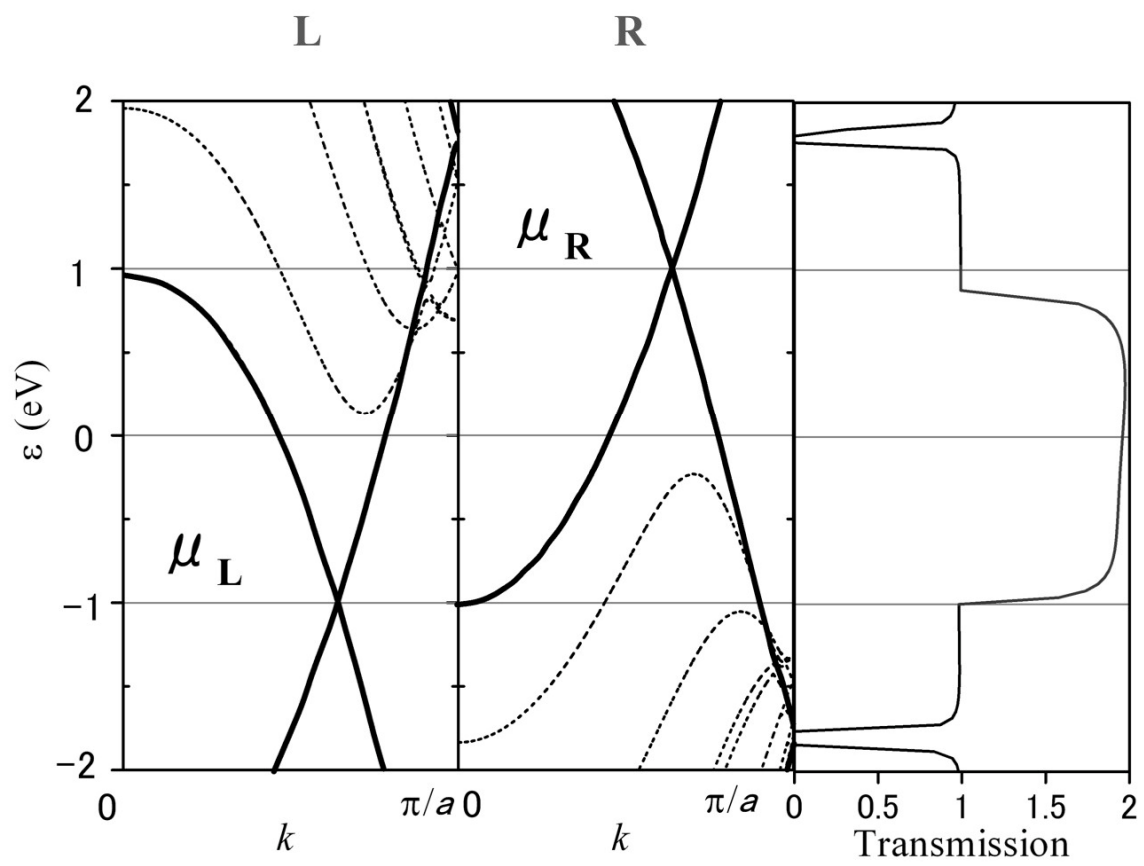


Figure 7

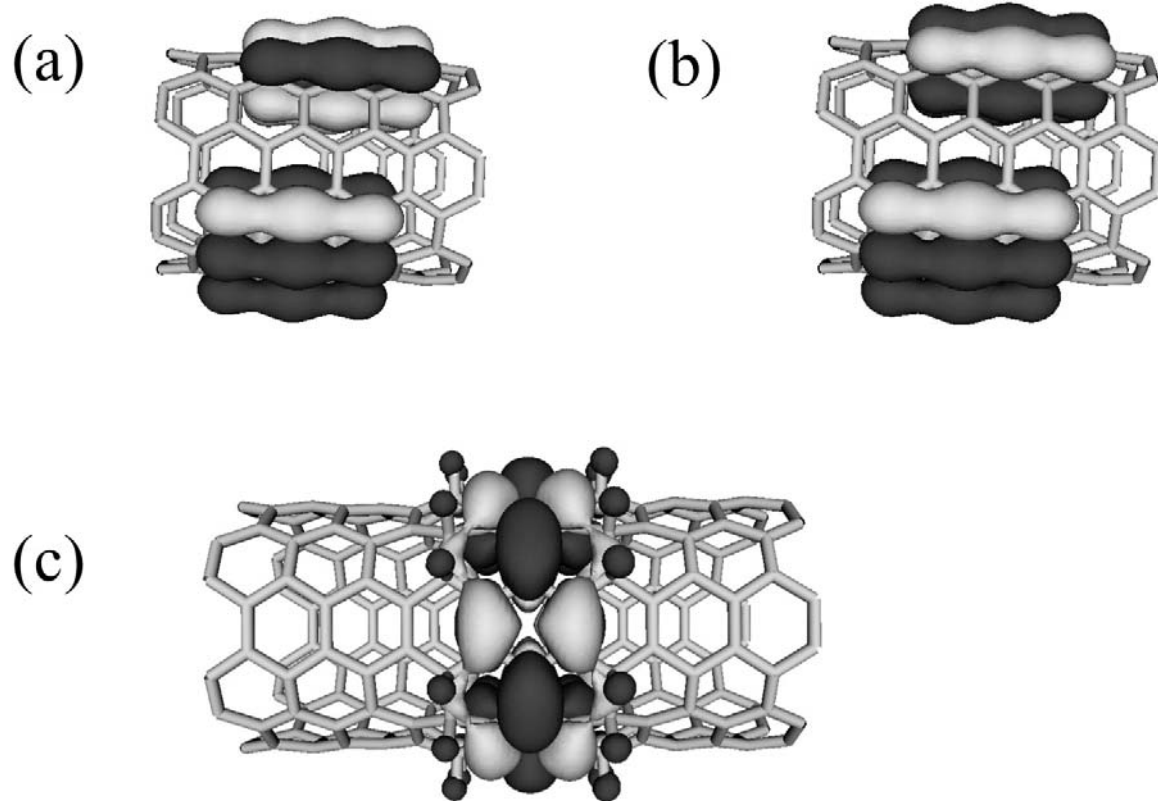


Figure 8

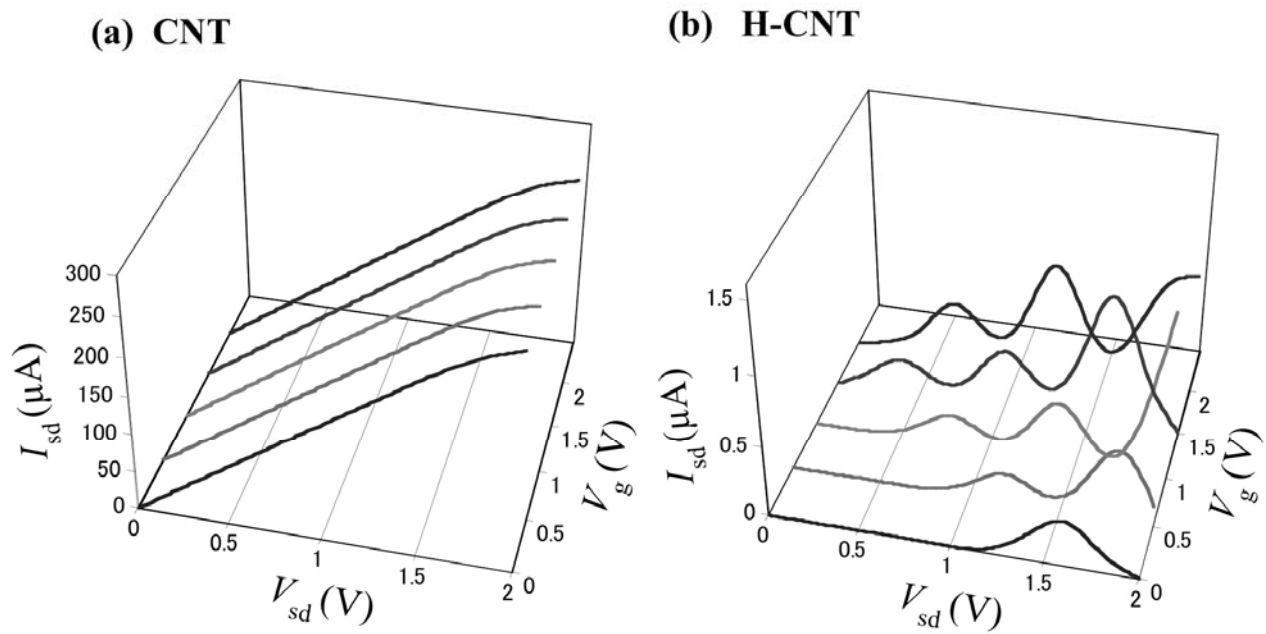


Figure 9

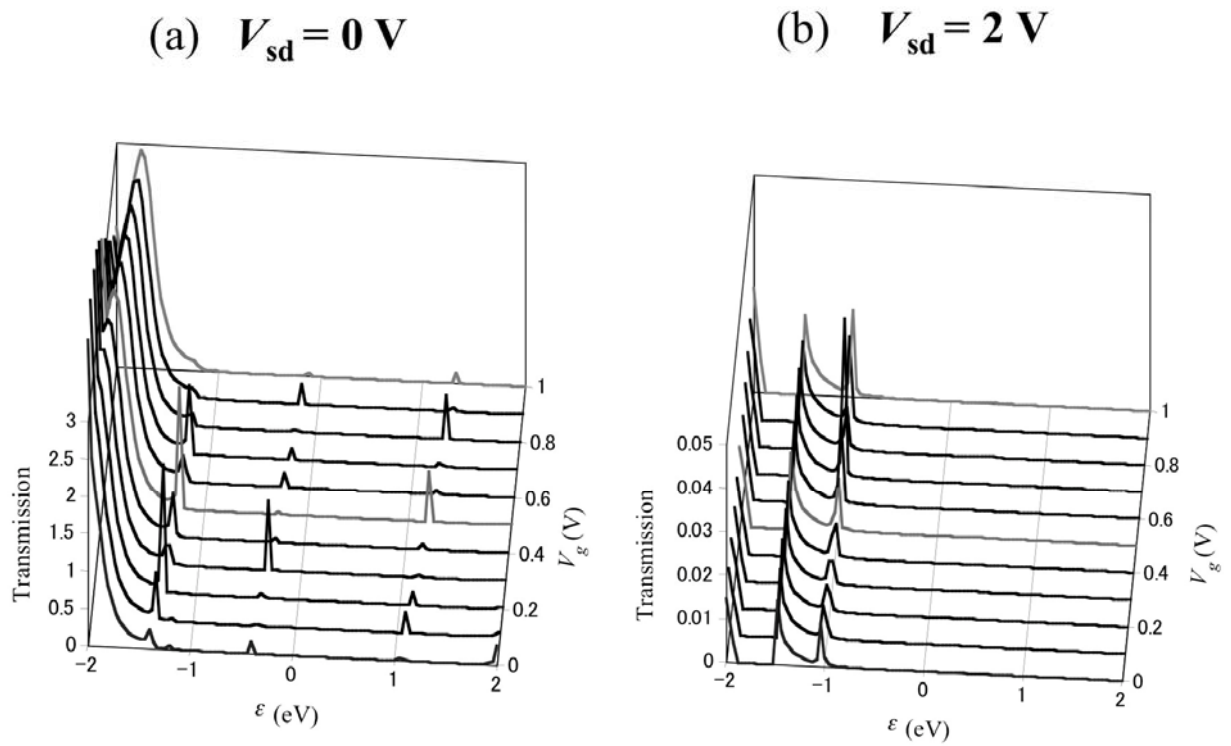


Figure 10

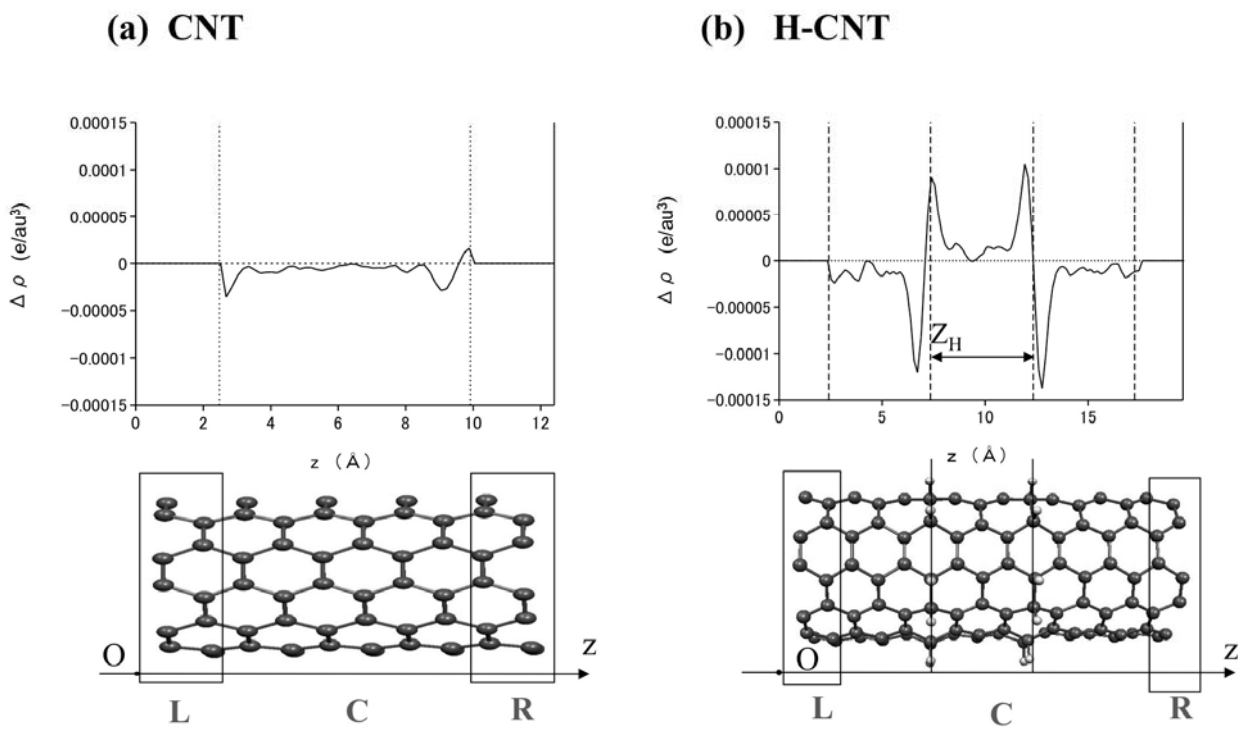


Figure 11